Quantitation and Localization of Matrix Metalloproteinases and Their Inhibitors in Human Carotid Endarterectomy Tissues

Salman Choudhary, Catherine L. Higgins, Iou Yih Chen, Michael Reardon, Gerald Lawrie, G. Wesley Vick III, Christof Karmonik, David P. Via, Joel D. Morrisett

Background—Matrix metalloproteinases (MMPs) and their inhibitors (TIMPs) play a central role in arterial wall remodeling, affecting stability of fibrous caps covering atherosclerotic plaques. The objective of this study was to determine the spatial distribution of TIMP mass and MMP mass and activity of carotid endarterectomy (CEA) tissues and relate it to the distribution of atherosclerotic lesions.

Methods and Results—Fresh CEA tissues were imaged by multicontrast MRI to generate 3D reconstructions. Tissue segments were cut transversely from the common, bifurcation, internal, and external regions. Segments were subjected to total protein extractions and analyzed by ELISA for MMP-2 and -9 and TIMP-1 and -2 mass and by zymography for gelatinase activity. Segments at or near the bifurcation with highly calcified lesions contained higher MMP levels and activity than segments distant from the bifurcation; highly fibrotic or necrotic plaque contained lower MMP levels and activity and higher TIMP levels. Fatty streak, fibroatheroma with hemorrhage and calcification, and fully occluded lesions were enriched in MMP-2, MMP-9, and TIMP-1 and TIMP-2, respectively.

Conclusion—The spatial distribution of MMPs and TIMPs in carotid atherosclerotic lesions is highly heterogeneous, reflecting lesion location, size, and composition. This study provides the first semi-quantitative maps of differential distribution of MMPs and TIMPs over atherosclerotic plaques. (***Arterioscler Thromb Vasc Biol*. 2006;26:2351-2358.)**

Key Words: carotid artery ■ atherosclerosis ■ MMPs ■ TIMPs ■ MRI

Downloaded from http://ahajournals.org by on April 5, 2021

Advanced atherosclerotic plaques typically have a lipid-rich core covered by a fibrous cap composed of smooth muscle cells (SMC) and extracellular matrix (ECM).[1] Plaque vulnerability is influenced by overall size, core size, cap thickness, cap inflammation, and cap fatigue. Fibrous caps are composed mainly of collagen, which determines cap tensile strength.[2] Matrix composition affects several events in lesion development, including cell migration and proliferation, lipoprotein retention, cell adhesion, calcification, thrombosis, and apoptosis.[3]

See page 2181 and cover

Degradation of ECM, which may weaken the fibrous cap resulting in plaque rupture, can be accomplished by macrophages through phagocytosis or secreted proteolytic enzymes, such as matrix metalloproteinases (MMPs).[4] MMPs are a family of Zn^{2+}- and Ca^{2+}-dependent endopeptidases that degrade ECM proteins, such as gelatin, collagen, elastin, and fibrin, and play a central role in arterial wall remodeling. Secreted as zymogens (pro-MMPs) that must be activated by other proteases or reaction with organic mercurials, MMPs are active at neutral pH and can be inhibited by proteins including tissue inhibitors of metalloproteinases (TIMPs), by α_2-macroglubulin, and by metal chelators such as phenanthroline and EDTA.[5,6] Although the MMP family consists of almost 20 known proteins, the present study has focused on MMP-2 and -9 and their role in carotid atherosclerosis.

MMP-2 (gelatinase A) is secreted as a 72-kDa proenzyme and primarily expressed in mesenchymal cells during development and tissue regeneration.[7] Cleaving the N-terminal prodomain can be initiated by membrane-type MMPs or serine proteases.[8] MMP-2 can degrade collagens, elastin, and fibronectin. With MMP-9, it degrades type IV collagen, the major component of basement membranes and gelatin.

MMP-9 (gelatinase B) has been identified in a number of cell types and has a broad range of specificities for native collagens, as well as gelatin, proteoglycans, and elastin. Secreted in a precursor form (pro–MMP-9, 92 kDa) that can be activated by MMP-3 (stromelysin-1) or bacterial proteinases, MMP-9 has been implicated in processes characteristic of inflammatory cells, uterine invasion of trophoblasts, and bone absorption and is thought to act synergistically with

Original received February 27, 2006; final version accepted June 21, 2006.

From the Departments of Medicine and Biochemistry and Molecular Biology (S.C., C.L.H., I.Y.C., D.P.V., J.D.M.), Baylor College of Medicine; The Methodist Hospital (M.R., G.L.); Department of Pediatrics (G.W.V.), Texas Children's Hospital; and Department of Radiology (C.K.), The Methodist Hospital Research Institute, Houston, Tex.

S.C. and C.L.H. contributed equally to this work.

Correspondence to Dr Joel D. Morrisett, The Methodist Hospital, A-601, 6565 Fannin St, Houston, TX 77030. E-mail morriset@bcm.tmc.edu

© 2006 American Heart Association, Inc.

Arterioscler Thromb Vasc Biol. **is available at http://www.atvbaha.org** **DOI: 10.1161/01.ATV.0000239461.87113.0b**

MMP-1 in degradation of fibrillar collagens as it degrades their denatured gelatin forms.[9,10] Expressed by almost all activated macrophages, MMP-9 is the most prevalent form of MMP.

The natural plasma inhibitors of MMPs are TIMPs, which act to suppress matrix degradation and can be synthesized by monocytes/macrophages, SMC, and endothelial cells. Tissue activity requires a balance between MMP activation and TIMP inhibition, which is important in tissue remodeling, inflammation, tumor growth, and metastasis. TIMPs form 1:1 noncovalent complexes with MMPs and block access of substrates to catalytic sites. Four members of the TIMP family are known, 2 of which, TIMP-1 and -2, are part of this study focus.

Dysregulation of MMP/TIMP balance is a characteristic of extensive tissue degradation in certain degenerative diseases. Secretion of proteases at focal sites in plaques ultimately results in plaque instability and rupture. Therefore, localizing MMPs and TIMPs in atherosclerotic lesions is necessary for understanding the disease progression and regression.

MRI has become a powerful technology for imaging carotid atherosclerotic lesions in vivo. MRI was used to demonstrate that lipid-lowering with simvastatin is associated with significant regression of human carotid atherosclerotic lesions[11] and to show that substantial low-density lipoprotein cholesterol reduction with rosuvastatin resulted in regression of lipid-rich necrotic core.[12] Takaya et al[13] demonstrated by MRI that hemorrhage into plaque accelerated progression. These and earlier studies[14] attest to the value of MRI as a noninvasive method for accurately monitoring plaque dimensions (total vessel volume, normal wall volume, plaque volume, lumen volume) and composition (calcification, lipid, fibrous, thrombus).

Downloaded from http://ahajournals.org by on April 5, 2021

Materials and Methods

Tissue Acquisition and Storage

Carotid endarterectomy (CEA) specimens were obtained within 1 hour after surgical resection, digitally photographed, and stored until use in 50% glycerol/PBS (20°C) to preserve tissue morphology. Larger specimens having intact common, internal, and external branches were preferred for study (approved by an institutional review committee of Baylor College of Medicine; subjects gave informed consent).

Magnetic Resonance Imaging

Tissues were washed in PBS and transferred to a specially fabricated sample holder, permitting simultaneous imaging of 4 samples.[15] The holder oriented the tissue long axis along the y-axis of the magnet so that 2-mm coronal slices gave axial images (supplemental Figure I, available online at http://atvb.ahajournals.org). A General Electric XL Enhance system operating at 1.5 T equipped with 6-cm phased array coils (Pathway Biomedical, Redmond, Wash) was used to acquire proton density weighted (PD-W), T1 weighted (T1W), and T2 weighted (T2W) images under conditions similar to those described previously.[16]

Tissue Segmentation and Digital Photography

CEA specimens were cut into 5-mm segments from the bifurcation into the common, external, and internal carotids. Microscopic images of segments were acquired using a Leica DC300 digital camera attached to a Stereomaster dissecting microscope to document features frequently lost during processing (eg, thrombus, calcification) and to capture subtle textural and morphological features not always detected by other techniques. Using these images, lesion composition was evaluated and lesion categories were assigned.[17]

Protein Extraction

Tissues were extracted for total protein by the following methods.

Mild Conditions

Tissue segments (tissue nos. 958, 973, 974, 991, 1006) were transferred to tared 15-mL plastic culture tubes and weighed. Segments were then incubated with 2 mL of DMEM containing 4 μL of gentamycin (50 μg/100 mL) while agitated gently at room temperature for 15 hours, after which the extract medium was removed and stored (−20°C) for analysis.

Moderate Conditions

Moderate conditions sequentially followed mild conditions. Tissue segments (tissue nos. 958, 973, 974, 991, 1006) were transferred to tared 15-mL plastic culture tubes and weighed. To each tube was added 3 mL of DMEM containing 6 μL of gentamycin (50 μg/100 mL) and 0.1% octyl glucoside. Tissues were homogenized (Brinkmann Polytron; 10-second bursts, 50% power) until segments were completely dispersed into homogeneous suspensions. Extensively calcified tissues required multiple homogenization bursts. Homogenates were centrifuged at 3000 rpm (30 minutes). Supernatants were decanted into cryovials and stored (−20°C) until analyzed.

Stringent Conditions

Tissues (tissue nos. 960, 968, 985, 989, 1000) were transferred to tared 15-mL plastic culture tubes and weighed. To each tube was added 3 mL of extraction buffer (50 mmol/L 4-[2-hydroxyethyl]-1-piperazineethanesulfonic acid [HEPES], 150 mmol/L NaCl, 1 mmol/L ethylene glycol-bis[2-aminoethylether]-*N*,*N*,*N*′,*N*′-tetraacetic acid [EGTA], 10 mmol/L sodium pyrophosphate, 100 mmol/L NaF, 1.5 mmol/L $MgCl_2$, 10% glycerol, 1% Triton X-100 [pH 7.5]). Tissues were homogenized as described for moderate conditions.

Measurement of MMPs and TIMPs in Tissue Extracts

Human total MMP-2,[7,8] total MMP-9,[6,9,10] TIMP-1,[18,19] and TIMP-2[20,21] were measured by enzyme-linked immunosorbent assay (ELISA) with reagents from R&D Systems (Minneapolis, Minn) following the instructions in the product insert. MMP and TIMP data were normalized for extraction efficiency (supplemental Table I) and total protein and were expressed in normalized form unless otherwise stated. Proteins extracted under mild and moderate conditions were analyzed separately, and the individual data were added together.

Zymography

Zymography was performed on total protein extracts from CEA tissue segments. Zymograms were run on 10% gels containing gelatin (Bio-Rad, Richmond, Calif) using the procedure described in the package insert. After electrophoresis, gels were renatured by incubation in detergent-free buffer, then activated by equilibration in activation buffer (50 mmol/L Tris hydroxymethyl aminomethane [TRIS], 150 mmol/L NaCl, 10 mmol/L $CaCl_2$, 1 μmol/L $ZnCl_2$, 0.02% NaN_3, pH7.5; 37°C, 4 hours). Gels were stained with Coomassie blue (0.05%, 30 minutes). Areas in which gelatin was digested appeared as clear bands (supplemental Figure III). ImageJ software was used to quantify bands. Enzyme activity was expressed in terms of band area produced per nanogram of pure MMP-9 (Oncogene, Boston, Mass). A standard curve for each gel was generated from 0.25, 0.50, 1.00, and 2.00 ng of pure MMP-9. The area of each band was integrated individually and plotted on a histogram showing relative contribution to total gelatinase activity.

Three-Dimensional Reconstructions and MMP Data Fusion

Three-dimensional renderings of CEA tissues were generated using MRI slices by first interpolating the image data to contiguous slices

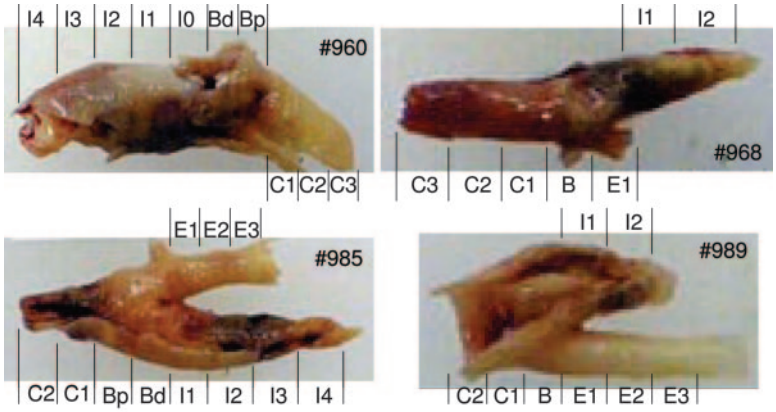

Figure 1. Digital photographs of human CEA tissues (nos. 960, 968, 985, 989) with demarcation lines indicating segment location and identity.

of 1-mm thickness as the lowest common denominator between the MRI slice thickness of 2 mm and the tissue segment thickness of 5 mm. The grayscale pixel values of the CEA tissue in each slice was then mapped to MMP enzyme activity in the following manner: MMP activity of 7 ng/mg total protein (as upper limit of MMP activity for all tissues) was assigned a grayscale value of 255. For each tissue segment (5 of the 1-mm slices), a grayscale value proportional to MMP activity was calculated by dividing the segment MMP activity by 7 and multiplying by 255. This modified image data were stored in raw image data format. All image manipulations were performed using the ImageJ software package developed by Wayne Rasband (Research Services Branch, National Institute of Mental Health, Bethesda, Md; http://rsb.info.nih.gov/ij). Next, the Paraview software package (http://www.paraview.org) was utilized to create 3D-surface rendered reconstructions with a color lookup table mapping the grayscale pixel value 0 to purple and the grayscale pixel value 255 to red.

Statistical Analysis

Plots indicating extent of association among MMP activity in CEA segment extracts (as determined by gelatin zymography) and MMP and TIMP masses (as determined by ELISA) were generated. The association between different analytes was determined by Spearman correlation analysis. Correlations with $P<0.05$ were considered statistically significant.

Results

The PD-W magnetic resonance (MR) images show discrete 2-mm slices (supplemental Figure II) corresponding to tissue contained within specific 5-mm segments (supplemental Figures IV through XIII). These images (32 slices acquired, 4 shown) capture features seen in macroscopic images of intact tissues (Figure 1) and microscopic images of segments (supplemental Figures IV through XIII). For example in tissue 960, slices 14 of 32 and 18 of 32, corresponding to segments I1 and Bd (supplemental Figure II), exhibit large hypointense stenotic regions attributable to calcification as verified by coregistered digital photographs (supplemental Figure V). These 2D MR images were used to reconstruct 3D images that served as templates onto which segment properties (eg, enzyme activity, protein mass) were mapped.

The MR images, macroscopic pictures, and microscopic photos each indicated considerable structural and compositional heterogeneity. Frequently, the bifurcation segment(s) had the greatest lesion burden, diminishing in the common and internal carotid segments with increasing distance from the flow divider. Typically, the external carotid contained little if any lesion and appeared as a patent, whitish tube (Figure 1: no. 985, E1 through E3; no. 989, E1 through E3). The high calcification content of some CEA tissues made it difficult to obtain histological sections that retained all the original components. For this reason, we used digital photography to document segment composition. The value of this approach is illustrated in supplemental Figure V, which shows extensive calcification in segments C1, Bp, Bd, and I0 (no. 960). The 3D visualization of this component is difficult if not impossible to duplicate by conventional histology of paraffin or frozen sections.

The heterogeneous distribution of macroscopic components suggested heterogeneous distribution of molecular components, such as MMPs and TIMPs. Rather than perform qualitative immunohistochemical staining for these proteins in situ, we chose to extract them from the tissue segments and analyze them by ELISA. This approach enabled quantitation of not only the individual proteins but also composite enzymatic activity. Three different extraction procedures were used. Forty segments cut from 5 CEA tissues (nos. 958, 973, 974, 991, 1006) were subjected first to the mild then moderate extraction procedure, and 42 segments cut from 5 tissues (nos. 960, 968, 985, 989, 1000) were subjected to the stringent procedure.

The effect of each extraction buffer on the immunoreactivity of each MMP and TIMP was determined by comparing the immunoreactivity of each pure protein before and after its exposure to the extraction buffer. Mild, moderate, and stringent buffers led to immunoreactivity recoveries of 88 to 97, 92 to 107, and 73% to 99%, respectively, for each MMP and TIMP (supplemental Table I).

The effect of the extraction process on MMPs and TIMPs was determined by measuring the percent recovery of immunoreactivity of exogenous protein added to normal CEA tissues subjected to one cycle of extraction. The process allowed recovery of 61 to 100, 81 to 107, and 61% to 118% immunoreactivity under mild, moderate, and stringent conditions, respectively (supplemental Table I).

The total extraction efficiency for MMPs and TIMPs was evaluated by measuring the immunoreactivity of endogenous protein in CEA tissue subjected to three extraction cycles, then extrapolating to 0 cycles. This measurement compensated for the effect of buffer and the extraction process on the

Downloaded from http://ahajournals.org by on April 5, 2021

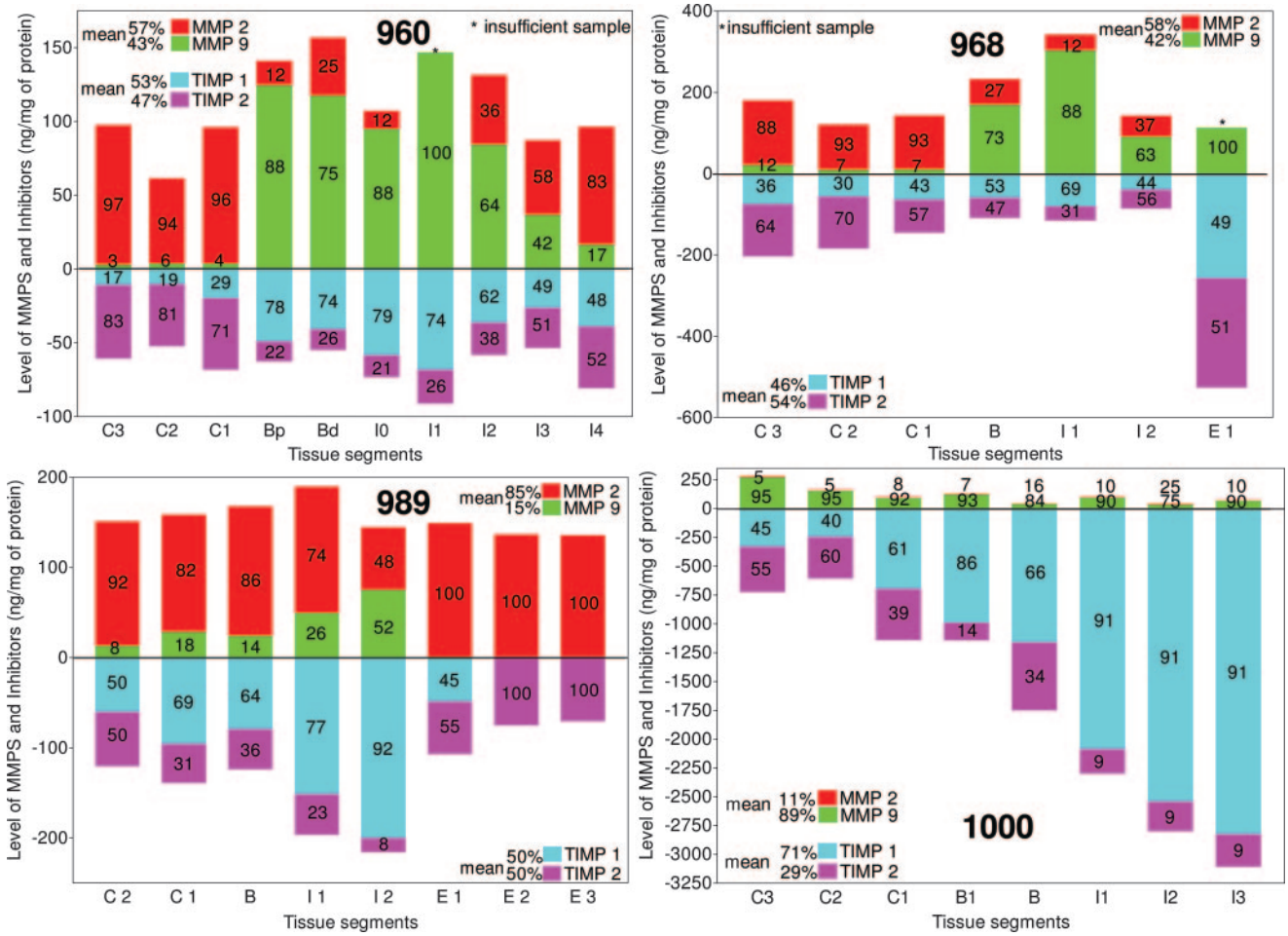

Figure 2. MMP and TIMP levels as determined by ELISA for the human CEA tissue segments (nos. 960, 968, 989, 1000), subjected to stringent extraction. MMP-2 and MMP-9 levels extend above the origin; TIMP-1 and TIMP-2 levels extend below the origin. Percentage of each MMP and TIMP level is indicated within each histogram.

total amount of MMPs and TIMPs measured by ELISA. The extraction efficiency for mild, moderate, and stringent buffers was 73 to 100, 69 to 100, and 68% to 100%, respectively (supplemental Table I).

The extraction efficiency values were used to correct the MMP and TIMP values measured by ELISA. Corrected values were plotted as positive histograms for MMP-2 and MMP-9 and as negative histograms for TIMP-1 and TIMP-2 (Figure 2). Each histogram represents the mass of these proteins as a function of tissue segment position.

Several of the tissues studied were highly calcified at or near the bifurcation (eg, supplemental Figure V; no. 960: I1, I0, Bd, Bp). These segments were rich in MMPs and poor in TIMPs (Figure 2). In other CEA tissues, the bifurcation was very fibrotic and/or necrotic (supplemental Figure XII; no. 1000: B1, B, I1, I2, I3). These segments were poorer in MMPs and richer in TIMPs, especially TIMP-1. In still other tissues, the bifurcation area contained a thrombus (supplemental Figure VI; no. 968: B, I1). These segments were also rich in MMPs, especially MMP-9 (Figure 2).

Although ELISA measurements of MMPs and TIMPs indicate absolute abundance of these proteins in tissue extracts, this information does not necessarily indicate net gelatinase activity operating on the tissue. This activity was determined by gelatin zymography.[22] Major bands, with molecular masses of 100 and 88 kDa, corresponding to MMP-9, and with 70 and 62 kDa, corresponding to MMP-2 were observed (supplemental Figure III). An additional band with a molecular mass of 130 kDa, not previously assigned to an individual MMP, was observed in some but not all extracts. The combined MMP-9 (or MMP-2) band areas for each extract sample were taken as a quantitative measure of MMP-9 (or MMP-2) activity. The MMP-9 activity, expressed as band area per unit MMP-9 mass, was significantly associated with MMP-9 abundance in some tissues (eg, nos. 960, 968, 973, 989, 1006) but not in others (eg, nos. 958, 965, 985, 991, 1000). Similarly, MMP-2 mass was also correlated with activity in some tissues (eg, nos. 958, 991, 1006) but not in others (eg, nos. 960, 968, 973, 974, 985, 989, 1000). This variability of statistically significant association between MMP-2 or MMP-9 mass and gelatinase activity in individual tissues may be due in part to the variation in TIMP-1 and TIMP-2 abundance. However, when the data from all ten tissues were combined, the mass of MMP-9 in individual tissue segment extracts was correlated ($r=0.61$, $P<0.0001$, n=42) with the activity of MMP-9. Likewise, the mass of MMP-2 was correlated ($r=0.43$, $P=0.004$, n=42) with activity of MMP-2.

Downloaded from http://ahajournals.org by on April 5, 2021

To enhance visualization of gelatinase activity distribution over the CEA tissues, total activity values (0 to 7 MMP-9 ng equivalents) were color-coded then mapped onto 3D reconstructions of tissue nos. 960, 968, 985, 989. These representations indicate that maximum activity is localized to diseased segments at or near the bifurcation including the common and internal but not the external carotid.

Discussion

CEA tissues are highly heterogeneous, containing some areas that are grossly normal and other areas that are extensively stenosed. By cutting the common, internal, and external carotid branches into multiple segments, we were able to isolate normal and diseased regions and characterize their morphology, dimensions, and composition (Figure 1).

The conventional approach for characterizing atherosclerotic plaque morphology has been histological analysis of paraffin or frozen sections. However, many CEA tissues are so structurally fragile that they are not amenable to this approach. For this reason, we elected to use digital photography to capture images that showed features often lost during sectioning and staining procedures.

Immunohistochemistry is extensively used for depicting distribution of specific proteins in tissues. However, the results are usually qualitative and do not readily allow reasonably accurate quantitation. Because we wanted to quantitatively compare several different protein components in the same tissue segment, we chose to perform total protein extraction on each segment, then measure analytes of choice in the extract. When accompanied by careful controls, the total extract approach enables measurement of selected protein mass and activity by ELISA and zymography, respectively. In a separate study, we have used these extracts for protein microarray analysis.[23]

In the present study, we have used 2D MR image slices to reconstruct 3D images of the tissues. These 3D images serve as useful templates onto which specific molecular components (eg, protein, mRNA) can be quantitatively mapped, a capability not available from 2D digital photographs.

In this study, 10 CEA tissues were cut into ≈80 segments that were characterized in terms of morphology, MMP and TIMP composition, and gelatinase activity. Segments at or adjacent to the bifurcation were significantly stenosed, containing varying amounts of lipid, thrombus, calcification, and/or fibrotic material. The accumulation of these plaque components is usually attended by arterial remodeling, a process mediated by MMPs and attenuated by TIMPs. Typically, the abundance of MMPs was greatest in lesioned segments at the bifurcation (eg, Bp, Bd) or adjacent to it (eg, I1). MMP-9 was frequently the most abundant MMP, up to 95% in some segments, but occasionally MMP-2 was predominant (Figure 2; no. 989). In grossly normal segments such as those in the external carotid (Figure 1; no. 989: E1 through E3) and proximal common carotid (Figure 1; nos. 960, 968: C1 through C3), the abundance of MMPs was significantly less than in lesioned segments, suggesting that the normal segments were not undergoing as extensive remodeling as lesioned segments. Notably, the greater abundance of MMP-9 in the plaque area suggests that it is a major MMP mediating remodeling in this area. In grossly normal areas, the level of total MMPs is lower and dominated by MMP-2. This observation suggests that remodeling of atheroma and normal arterial wall are mediated by different MMPs.[24,25] The relative mass abundance of each MMP suggests but does not prove relative proteinase activity. This issue was addressed by gelatin zymography (supplemental Figure III), which demonstrated that the mass of MMP-9 protein measured by ELISA was significantly associated with gelatinase activity of MMP-9 ($r=0.614$) and that MMP-2 protein mass was correlated with MMP-2 activity ($r=0.435$). Proteinase activity was highest in lesioned segments (eg, Figure 3; no. 960: Bd, Bp) containing abundant MMPs and was somewhat lower in most normal segments (eg, Figure 3; no. 989: E1 through E3).

This study clearly demonstrates the longitudinal heterogeneous distribution of MMPs and TIMPS among atherosclerotic lesions and grossly normal regions within 5-mm tissue segments. However, this interplane spatial resolution does not enable qualitative description nor quantitative measurement of subtle intraplane differences. The circumferential rings of artery may contain both diseased and healthy regions, and the combination of these 2 may account for some of the variability in our results. Such differences will require higher resolution techniques such as thin section microscopy, laser capture microdissection, and protein microarrays for ultrastructural description and analysis.

The American Heart Association Committee on Vascular Lesions[26] and Virmani et al[17] have developed a system for classifying lesions according to their morphological and compositional features from 2D histological thin sections of coronary lesions. In this study, we have used digital images that contained significant 3D information and MRI, which can distinguish plaque components,[27] to classify the lesions in CEA segments (supplemental Table II). Many segments in the external and proximal common carotid exhibited mild fibrous or lipid accumulation and were classified as types I to III. Most of the segments in the bifurcation and proximal internal carotid contained large fibroatheroma frequently with hemorrhage and/or calcification and hence were classified as type IVa. This lesion was the most abundant (36%) of all the 10 types, with IVb being the next most abundant (15%). Significantly, the type II lesions contained more MMP-2 than any other lesion type, whereas type IVc lesions contained the most MMP-9, suggesting that type IVc lesions are undergoing considerable remodeling (Figure 4). Lesion type Vd contained much greater amounts of TIMP-1 and TIMP-2 than any other lesion type. This finding suggests that type Vd lesions have depressed MMP activity and suppressed remodeling, leading to net formation of connective tissue and almost complete occlusion (supplemental Figure XII; no. 1000: B1, I1, I2).

Mapping total gelatinase activity on 3D CEA images reconstructed from 2D MRI slices provides a graphical method for efficiently conveying quantitative information (Figure 5). Tissue nos. 960 and 989 had the highest level of activity (≈7 MMP-9 ng equivalents); this activity was concentrated in the highly lesioned bifurcation and adjacent

Downloaded from http://ahajournals.org by on April 5, 2021

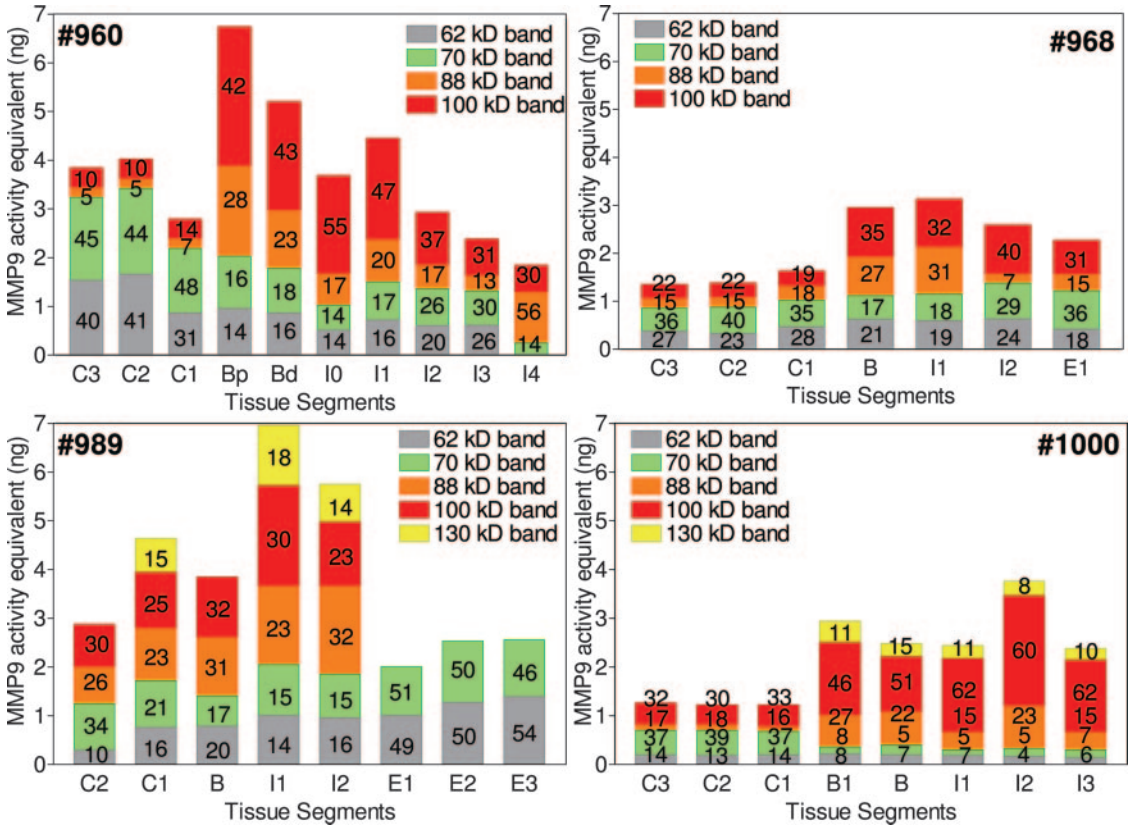

Figure 3. MMP activity reported as the activity displayed by 1 ng of pure MMP-9 and as determined by gelatin zymography for human CEA tissue segments (nos. 960, 968, 989, 1000). As many as 5 bands (62, 70, 88, 100, 130 kDa) were observed in some cases and all are displayed. Percentages of total MMP activity for each band are indicated.

Downloaded from http://ahajournals.org by on April 5, 2021

segments. Tissues with lower levels of activity still exhibited their maximal amount at or near the bifurcation.

Intraplaque hemorrhage is common in advanced coronary atherosclerotic lesions.[28] Significantly, hemorrhage has been shown to increase expression of MMPs, including MMP-2 and MMP-9, in lesions.[29] In the present study, a number of carotid atheroma segments exhibited sites of intraplaque hemorrhage (eg, supplemental Figure V: no. 968, Bd, I1, I2; supplemental Figure X: no. 989, C2, C1, B). These segments contained considerable amounts of MMP-2 and MMP-9 (Figure 2). The accumulation of MMPs at these sites may be attributable in part to the infiltration of macrophages, cells known to secrete MMPs and destabilize plaques.

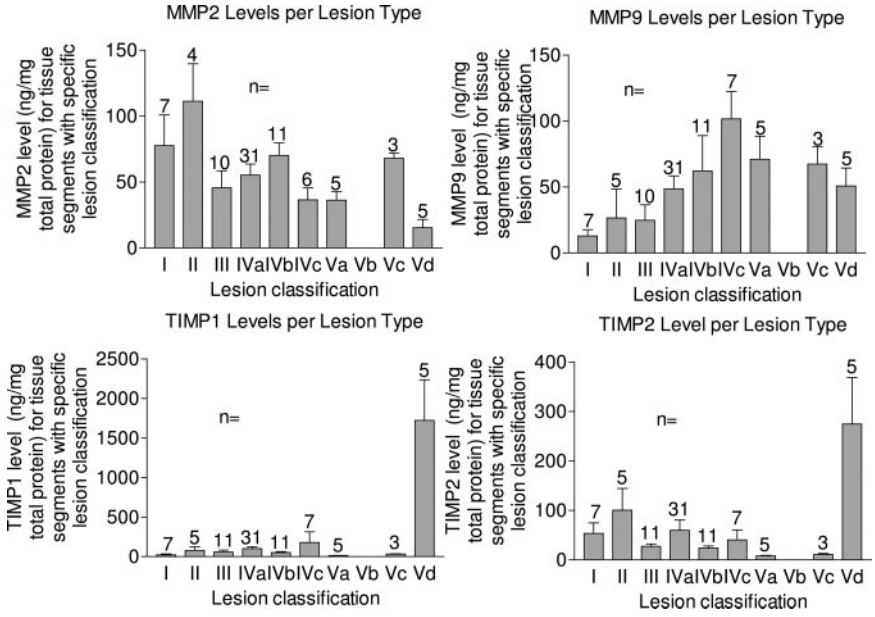

Figure 4. Distribution of MMP-2, MMP-9, TIMP-1, and TIMP-2 among CEA segments characterized by the lesion classification system developed by the American Heart Association Committee on Vascular Lesions[26] and Virmani et al.[17] Type II lesions contained the most MMP-2. Type IVc lesions had the highest content of MMP-9. Type Vd lesions contained the most TIMP-1 and TIMP-2. Histogram height represents the mean level of a specific MMP found in a particular lesion type.

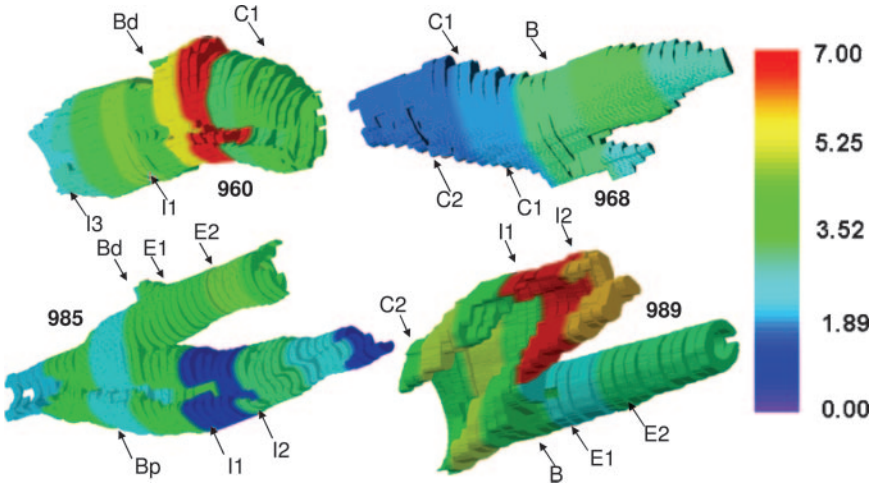

Figure 5. Three-dimensional reconstructions of CEA tissues (Figure 1) from multiple 2D MRI slices (supplemental Figure II; corresponding arrows) with fusion of MMP enzyme activity (Figure 3). Color-coded activity data were fused onto 3D renderings as described in the Materials and Methods. The maximal MMP activities from which the color levels were calibrated for tissue nos. 960, 968, 985, and 989 were 6.75, 3.12, 3.55, and 6.96 ng/mg total extracted protein, respectively.

The increasing body of evidence indicating the correlation of MMP and TIMP tissue levels with plaque stability[30,31] raises the question of how plasma levels of these proteins might be involved. This question has been addressed in a recent study by Sapienza et al[32] of MMP-1, -2, and -9 and TIMP-1 and -2 levels in patients undergoing endarterectomy. The plaques from patients were classified histologically as stable or unstable and their plasma MMP levels measured before and after surgery. Plasma MMP levels were higher in patients with unstable plaques compared with patients with stable plaques. In contrast, plasma levels of TIMPs were lower in patients with unstable plaques compared with stable plaques. This observation indicates that plasma levels of MMPs and TIMPs may be important biomarkers for carotid plaque instability.

Numerous studies have demonstrated that MMP-2 and MMP-9 are essential for SMC behavior and hence play a major role in fibrous cap formation and healing. However, imbalance in tissue levels of MMPs and TIMPs may be a cause of plaque instability. This condition might be treated by decreasing the level or activity of the enzymes. A feasible approach has been suggested by Bellosta et al,[33] who have observed that 3-hydroxy-3-methylglutaryl–coenzyme A (HMG-CoA) reductase inhibitors decrease MMP-9, an effect mediated by suppressing synthesis of mevalonate, a precursor of multiple intermediates essential for several cellular functions. Other approaches might include intervention with novel inhibitors of MMP gene expression or activity.

Conclusion

CEA tissue segments have been used to investigate the distribution and abundance of MMPs and TIMPs in atherosclerotic plaques. MMP-9 was highly abundant in calcified segments at or near the bifurcation. MMP-9 was very abundant in segments with intraplaque hemorrhage. Grossly normal segments contained lesser amounts of MMPs, which were predominantly MMP-2. TIMPs were lowly abundant in calcified plaques and more highly abundant in fibrotic and necrotic segments. This study provides the first semiquantitative maps of differential distributions of MMPs and TIMPs over an atherosclerotic plaque.

Downloaded from http://ahajournals.org by on April 5, 2021

Acknowledgments

We thank Seth Marvel for assistance with zymogram analysis.

Sources of Funding

This work has been supported in part by National Institutes of Health grants R01HL63090 and T32HL07812. (TTGA)

Disclosures

None.

References

1. Ross R. The pathogenesis of atherosclerosis: a perspective for the 1990s. *Nature.* 1993;362:801–809.
2. Burleigh MC, Briggs AD, Lendon CL, Davies MJ, Born GV, Richardson PD. Collagen types I and III, collagen content, GAGs and mechanical strength of human atherosclerotic plaque caps: span-wise variations. *Atherosclerosis.* 1992;96:71–81.
3. Wight TN. The extracellular matrix and atherosclerosis. *Curr Opin Lipidol.* 1995;6:326–334.
4. Dollery CM, McEwan JR, Henney AM. Matrix metalloproteinases and cardiovascular disease. *Circ Res.* 1995;77:863–868.
5. Massova I, Kotra LP, Fridman R, Mobashery S. Matrix metalloproteinases: structures, evolution, and diversification. *FASEB J.* 1998;12:1075–1095.
6. Birkedal-Hansen H, Moore WG, Bodden MK, Windsor LJ, Birkedal-Hansen B, DeCarlo A, Engler JA. Matrix metalloproteinases: a review. *Crit Rev Oral Biol Med.* 1993;4:197–250.
7. Morgunova E, Tuuttila A, Bergmann U, Isupov M, Lindqvist Y, Schneider G, Tryggvason K. Structure of human pro-matrix metalloproteinase-2: activation mechanism revealed. *Science.* 1999;284:1667–1670.
8. Nguyen M, Arkell J, Jackson CJ. Activated protein C directly activates human endothelial gelatinase A. *J Biol Chem.* 2000;275:9095–9098.
9. Ogata Y, Pratta MA, Nagase H, Arner EC. Matrix metalloproteinase 9 (92-kDa gelatinase/type IV collagenase) is induced in rabbit articular chondrocytes by cotreatment with interleukin 1 beta and a protein kinase C activator. *Exp Cell Res.* 1992;201:245–249.
10. Koide H, Nakamura T, Ebihara I, Tomino Y. Increased mRNA expression of metalloproteinase-9 in peripheral blood monocytes from patients with immunoglobulin A nephropathy. *Am J Kidney Dis.* 1996;28:32–39.
11. Corti R, Fuster V, Fayad ZA, Worthley SG, Helft G, Smith D, Weinberger J, Wentzel J, Mizsei G, Mercuri M, Badimon JJ. Lipid lowering by simvastatin induces regression of human atherosclerotic lesions: two years' follow-up by high-resolution noninvasive magnetic resonance imaging. *Circulation.* 2002;106:2884–2887.
12. Saam T, Yuan C, Zhao XQ, Takaya N, Underhill H, Chu B, Cai J, Kerwin W, Kraiss LW, Parker DL, Hamar W, Raichlen J, Cain V, Waterton J, Hatsukami TS. 75th European Atherosclerosis Society Congress, 2005, Prague, Czech Republic.
13. Takaya N, Yuan C, Chu B, Saam T, Polissar NL, Jarvik GP, Isaac C, McDonough J, Natiello C, Small R, Ferguson MS, Hatsukami TS.

Presence of intraplaque hemorrhage stimulates progression of carotid atherosclerotic plaques: a high-resolution magnetic resonance imaging study. *Circulation.* 2005;111:2768–2775.
14. Adams GJ, Greene J, Vick GW 3rd, Harrist R, Kimball KT, Karmonik C, Ballantyne CM, Insull W Jr, Morrisett JD. Tracking regression and progression of atherosclerosis in human carotid arteries using high-resolution magnetic resonance imaging. *Magn Reson Imaging*. 2004;22: 1249–1258.
15. Karmonik C, Adams G, Morrisett JD. Medical Imaging I: Vascular Imaging. 20th Annual Meeting of the Houston Society for Engineering in Medicine and Biology, 2003, Houston, Tex.
16. Adams GJ, Simoni DM, Bordelon CB Jr, Vick GW 3rd, Kimball KT, Insull W Jr, Morrisett JD. Bilateral symmetry of human carotid artery atherosclerosis. *Stroke*. 2002;33:2575–2580.
17. Virmani R, Kolodgie FD, Burke AP, Farb A, Schwartz SM. Lessons from sudden coronary death: a comprehensive morphological classification scheme for atherosclerotic lesions. *Arterioscler Thromb Vasc Biol.* 2000; 20:1262–1275.
18. Murphy G, Houbrechts A, Cockett MI, Williamson RA, O'Shea M, Docherty AJ. The N-terminal domain of tissue inhibitor of metalloproteinases retains metalloproteinase inhibitory activity. *Biochemistry.* 1991; 30:8097–8102.
19. Murphy G, Koklitis P, Carne AF. Dissociation of tissue inhibitor of metalloproteinases (TIMP) from enzyme complexes yields fully active inhibitor. *Biochem J.* 1989;261:1031–1034.
20. Brew K, Dinakarpandian D, Nagase H. Tissue inhibitors of metalloproteinases: evolution, structure and function. *Biochim Biophys Acta.* 2000; 1477:267–283.
21. Wang Z, Juttermann R, Soloway PD. TIMP-2 is required for efficient activation of proMMP-2 in vivo. *J Biol Chem.* 2000;275:26411–26415.
22. Snoek-van Beurden PA, Von den Hoff JW. Zymographic techniques for the analysis of matrix metalloproteinases and their inhibitors. *Biotechniques.* 2005;38:73–83.
23. Ramaswamy A, Lin E, Chen I, Mitra R, Morrisett J, Coombes K, Ju Z, Kapoor M. Application of protein lysate microarrays to molecular marker verification and quantification proteome. *Proteome Sci.* 2005;3:9.
24. Johnson C, Galis ZS. Matrix metalloproteinase-2 and -9 differentially regulate smooth muscle cell migration and cell-mediated collagen organization. *Arterioscler Thromb Vasc Biol.* 2004;24:54–60.
25. Rodriguez-Pla A, Bosch-Gil JA, Rossello-Urgell J, Huguet-Redecilla P, Stone JH, Vilardell-Tarres M. Metalloproteinase-2 and -9 in giant cell arteritis: involvement in vascular remodeling. *Circulation.* 2005;112: 264–269.
26. Stary HC, Chandler AB, Dinsmore RE, Fuster V, Glagov S, Insull W Jr, Rosenfeld ME, Schwartz CJ, Wagner WD, Wissler RW. A definition of advanced types of atherosclerotic lesions and a histological classification of atherosclerosis. A report from the Committee on Vascular Lesions of the Council on Arteriosclerosis. *Circulation.* 1995;92:1355–1374.
27. Higgins CL, Marvel SA, Morrisett JD. Quantification of calcification in atherosclerotic lesions. *Arterioscler Thromb Vasc Biol.* 2005;25: 1567–1576.
28. Kolodgie FD, Gold HK, Burke AP, Fowler DR, Kruth HS, Weber DK, Farb A, Guerrero LJ, Hayase M, Kutys R, Narula J, Finn AV, Virmani R. Intraplaque hemorrhage and progression of coronary atheroma. *N Engl J Med.* 2003;349:2316–2325.
29. Power C, Henry S, Del Bigio MR, Larsen PH, Corbett D, Imai Y, Yong VW, Peeling J. Intracerebral hemorrhage induces macrophage activation and matrix metalloproteinases. *Ann Neurol.* 2003;53:731–742.
30. Bicknell CD, Peck D, Alkhamesi NA, Cowling MG, Clark MW, Goldin R, Foale R, Jenkins MP, Wolfe JH, Darzi AW, Cheshire NJ. Relationship of matrix metalloproteinases and macrophages to embolization during endoluminal carotid interventions. *J Endovasc Ther.* 2004;11:483–493.
31. Beaudeux JL, Giral P, Bruckert E, Bernard M, Foglietti MJ, Chapman MJ. Serum matrix metalloproteinase-3 and tissue inhibitor of metalloproteinases-1 as potential markers of carotid atherosclerosis in infraclinical hyperlipidemia. *Atherosclerosis.* 2003;169:139–146.
32. Sapienza P, di Marzo L, Borrelli V, Sterpetti AV, Mingoli A, Cresti S, Cavallaro A. Metalloproteinases and their inhibitors are markers of plaque instability. *Surgery.* 2005;137:355–363.
33. Bellosta S, Via D, Canavesi M, Pfister P, Fumagalli R, Paoletti R, Bernini F. HMG-CoA reductase inhibitors reduce MMP-9 secretion by macrophages. *Arterioscler Thromb Vasc Biol.* 1998;18:1671–1678.

Downloaded from http://ahajournals.org by on April 5, 2021